Analysis of PM eddy current loss in rotor-PM and stator-PM flux-switching machines by air-gap field modulation theory

Su, P.; Hua, W.; Hu, M.; Chen, Zhe; Cheng, M.; Wang, W.

Published in:
IEEE Transactions on Industrial Electronics

DOI (link to publication from Publisher):
10.1109/TIE.2019.2902782

Publication date:
2020

Document Version
Accepted author manuscript, peer reviewed version

Analysis of PM eddy current loss in rotor-PM and stator-PM flux-switching machines by air-gap field modulation theory

Peng Su, *Student Member*, *IEEE*, Wei Hua, *Senior Member*, *IEEE*, Mingjin Hu, Zhe Chen, *Fellow*, *IEEE*, Ming Cheng, *Fellow*, *IEEE*, Wei Wang, *Member*, *IEEE*

***Abstract*—This paper investigates and compares the eddy current loss induced in permanent magnet (PM) in both rotor-PM flux-switching (RPM-FS) machines and stator-PM flux-switching (SPM-FS) machines. Based on the field modulation principle, the harmonic components of both the PM field and armature reaction field are deduced, as well as the corresponding frequencies. Then, the PM loss production mechanisms due to eddy current are revealed for the RPM-FS and SPM-FS machines, respectively. Consequently, the similarities and differences between two FS machines are investigated from the perspectives of both electromagnetic torque and PM eddy current loss production mechanisms. The results indicate that the PM eddy current loss in SPM-FS machines influences efficiency dramatically. However, for the RPM-FS machine, the armature reaction field affects the PM loss more sensitively. In addition, a large PM eddy current loss exhibits associated with high-power rating and large-current density FS machines for electric vehicle application, and it can be reduced by utilizing PM segmentation method.**

***Index Terms*—Flux switching, permanent magnet, PM eddy current loss, harmonic analysis, field modulation.**

NOMENCLATURE

A_{Wv}	Electrical loading of the armature winding harmonic component with v-pole-pair
$B_{gap}(\theta,t)$	Air-gap flux density distribution function due to PMs
$B_{Rw}(\theta,t)$	Air-gap flux density distribution function due to armature reaction
B_{gv}	v-order harmonic amplitude of magnetic loading
B_{smv}	v-order harmonic amplitude of PM flux density
D_{ro}	Rotor outer diameter
D_{si}	Stator inner diameter
D_{so}	Stator outer diameter
$F_{RPM}(\theta,t)$	The MMF distribution function due to rotor PMs
$F_{Rw}(\theta,t)$	The MMF distribution function due to armature reaction
$f_{\_PM}$	Mechanical frequency in PM coordinate system
f_{v_PM}	v-order harmonic frequency in PM coordinate system
g	Air-gap length
g_e	Effective air-gap length
HC	Harmonic components
h_{PM}	PM height
I_{Rmax}	The maximum value of phase armature current
k_{hPM}	PM height ratio
k_{hrt}	Rotor tooth height ratio
k_{sio}	Split ratio
$k_{PMloss/V}$	PM loss density
k_{PMloss}	PM loss ratio
l_a	Stack length
N_{Rc}	Coil turns number of RPM-FS machines
P_{PM}	Pole-pair number of PMs
P_{PMloss}	PM eddy current loss
P_r	Rotor pole-pair number
P_s	Stator slots number
T_e	Electromagnetic torque
w_{PM}	PM width
θ_0	Initial rotor position
ω_{r_PM}	Mechanical angular velocity in PM coordinate system
ω_{v_PM}	v-order harmonic electrical angular velocity in PM coordinate system
μ	Permeability of PMs
$\Lambda_{Rr}(\theta,t)$	Rotor core permeance distribution function
$\Lambda_s(\theta,t)$	Stator tooth permeance distribution function

Manuscript received Aug. 3, 2018; revised Dec. 1, 2018 and Jan. 22, 2019; accepted Feb. 14, 2019. This work was supported in part by the National Science Fund for Distinguished Young Scholars under Grant 51825701 and the Changjiang Scholars Program of China under Grant Q2017110. (*Corresponding author: Wei Hua.*)

Peng Su, Wei Hua, Mingjin Hu, Ming Cheng and Wei Wang are with the School of Electrical Engineering, Southeast University, Nanjing, 210096 China, (e-mail: supeng1639@126.com, huawei1978@seu.edu.cn, 1205195957@qq.com, mcheng@seu.edu.cn, and wangwei1986@seu.edu.cn).

Zhe Chen is with the Department of Energy Technology, Aalborg University, Aalborg 9220, Denmark (e-mail: zch@et.aau.dk).

I. INTRODUCTION

RECENTLY, stator permanent-magnet (PM) flux-switching (FS) (SPM-FS) machines have been considered as an attractive candidate for pure electric vehicles (PEVs) and hybrid electric vehicles (HEVs), due to the advantages of large torque density, high efficiency and robust rotor structure [1], [2]. However, since both PMs and armature windings coexist in the stator of SPM-FS machines, a significant reduction of

This article has been accepted for publication in a future issue of this journal, but has not been fully edited. Content may change prior to final publication. Citation information: DOI 10.1109/TIE.2019.2902782, IEEE Transactions on Industrial Electronics

electrical loadings and serious saturation in stator lamination limit the torque capability of SPM-FS machines [3]. Hence, rotor-permanent-magnet flux-switching (RPM-FS) machines were proposed to address the above issues, which evolves from the topology of the SPM-FS machines by removing PMs from stator to rotor to alleviate the space of armature windings [4]. Then, the electrical loading is enlarged and saturation releases considerably, and the improvement of torque capability can be obtained in RPM-FS machines [5].

Based on the field modulation principle, both the PM-excited and armature reaction-excited MMFs are modulated by the salient iron cores in the air-gap field. Then, the electromagnetic torque T_e is produced by the interaction between the harmonics of PM field and armature reaction field with the same order and rotation speed [6-8]. It is found that for the RPM-FS machines, T_e is dominantly contributed by the fundamental component with PM pole-pairs P_{PM}. However, for the SPM-FS machine, T_e is not only produced by the fundamental component but also attributed by the modulation harmonics [4], [9]. On the other hand, both the fundamental component and modulation harmonics in the air-gap field result in the PM flux density periodic variation, then the PM eddy current loss is generated.

The PM eddy current loss P_{PMloss} can be accurately deduced by the calculation model in [10], [11], which is helpful to obtain the efficiency of machines with different topologies. It is found that P_{PMloss} is mainly caused by the magnetic path variation of the armature reaction flux, and is dominantly determined by the electrical loading and its frequency [12]. For the machines used in PEV and HEV driving systems, the phase armature current density is relative large, e.g. the armature current density of the interior permanent magnet (IPM) machine in Toyota Prius 2004, Camry 2007 and Prius 2010, at maximum torque and base speed n_b is in excess of 20A/mm^2, and an oil cooling system is required [13]. Thus, it can be expected that the FS machines used for PEV and HEV applications will exhibit a large PM eddy current loss, causing the PM temperature rise and then improving the risk of partial demagnetization in PMs [5].

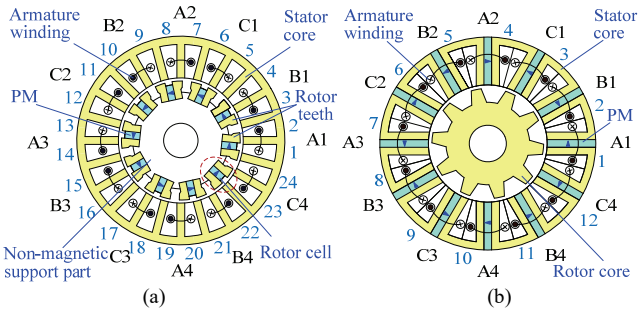

Fig. 1 The topologies of two flux-switching machines. (a) 24s/10p RPM-FS machine. (b) 12s/10p SPM-FS machine.

The purpose of this paper is to analyze and compare the production mechanism and performance influence of PM eddy current loss in the RPM-FS machine and the SPM-FS machine. The typical 12-slots/10-pole-pairs (12s/10p) SPM-FS machine and the 24-slots/10-pole-pairs (24s/10p) RPM-FS machine are chosen, as shown in Fig. 1, where the topology of the later is evolved from the former [4]. Firstly, based on the field modulation theory, the PM eddy current loss production mechanism is investigated, and the similarities and differences of PM loss harmonic contributions between the RPM-FS and SPM-FS machines are revealed in Section II. Then in Section III, a comparison of P_{PMloss} between two machines is conducted under two conditions, i.e. open-circuit no-load and rated on-load, respectively. Further, P_{PMloss} in high-power rating RPM-FS and SPM-FS machines are predicted and it can be concluded that P_{PMloss} in FS machines influences the efficiency dramatically, which can be reduced by the PM segmentations as arranged in Section IV. Finally, conclusions are drawn in Section V.

II. PM Loss Production Mechanism in FS Machines

Both RPM-FS and SPM-FS machines exhibit doubly salient structure, resulting in the PM and armature reaction air-gap fields containing complex harmonic components due to the salient iron cores modulation effect, in which part of harmonics contribute the P_{PMloss}. P_{PMloss} can be obtained by the model considering PM eddy current reaction effect as expressed in equation (1) [10], [11].

$$P_{PMloss}=\frac{32}{\pi^2}\cdot\left(\frac{g_e}{w_{PM}}\right)^2\cdot\sum_{n=1,3,5\ldots}\sum_{m=1,3,5\ldots}\frac{w_{PM}h_{PM}l_a\sigma\omega_{v\_PM}^2B_{smv}^2}{\left(\frac{g_e}{w_{PM}}\cdot\left(\frac{n\pi}{h_{PM}}\right)^2+\frac{g_e}{w_{PM}}\cdot\left(\frac{m\pi}{l_a}\right)^2\right)^2+\left(\omega_{v\_PM}\mu\sigma\right)^2}\cdot\left(\frac{1}{(l_a\cdot n)^2}+\frac{1}{(h_{PM}\cdot m)^2}\right) \tag{1}$$

where w_{PM}, h_{PM} and l_a are the width, length and axial length of PMs, respectively. σ and μ are the conductivity and permeability of PMs, respectively. g_e is the effective air-gap length, which is equal to $w_{PM}+g\mu_r$ [10], g is air gap length and μ_r is PM relative permeability. B_{smv} is the v-order harmonic amplitude of PM flux density, and ω_{v_PM} is the corresponding harmonic electrical angular speed relative to the PM.

Obviously, P_{PMloss} is mainly determined by B_{smv}, ω_{v_PM} and PM geometric parameters. Hence, the effective harmonic orders B_{smv} and the corresponding v-order harmonic frequency $f_{v\_PM}=2\pi/\omega_{v\_PM}$ relative to the PMs in two FS machines should be investigated first. In this section, a PM coordinate system, which is relatively static with PMs, is utilized to deduce the air-gap flux density harmonic orders producing P_{PMloss}, i.e. the v-order harmonic frequency satisfying $f_{v\_PM}\neq0$.

A. RPM-FS machine.

For the RPM-FS machine, based on the PM coordinate system, the PM-MMF/permeance model and stator air-gap permeance model are shown in Fig. 2, where the permeance of iron core is assumed infinite and the flux leakage is neglected. Since the PMs are considered to be static, the PM-MMF distribution in air-gap field can be expressed as:

$$F_{RPM}(\theta)=\sum_{n=1}^{\infty}F_{RPMn}\sin(nP_{PM}\theta) \tag{2}$$

where F_{RPMn} is the Fourier series coefficients, and n is 1, 2, 3…

Since the stator teeth rotate relatively with the rotor by an angular speed ω_{r_PM} in the PM coordinate system (Fig. 2(b)), the stator air-gap permeance can be expressed as:

This article has been accepted for publication in a future issue of this journal, but has not been fully edited. Content may change prior to final publication. Citation information: DOI 10.1109/TIE.2019.2902782, IEEE Transactions on Industrial Electronics

$$\Lambda_s(\theta,t)=\Lambda_{S0}+\sum_{k=1}^{\infty}\Lambda_{Sk}\cos[kP_s(\theta+\omega_{r\_PM}t+\theta_0)] \tag{3}$$

where Λ_{S0} and Λ_{Sk} are the Fourier series coefficients, k is 1, 2, 3... and θ_0 is the initial position. P_s is stator slots number.

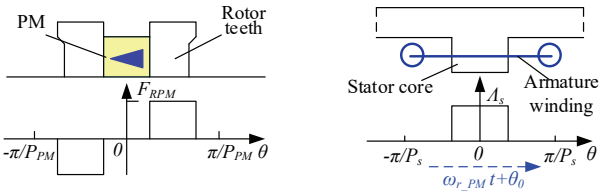

Fig. 2 The PM-MMF/permeance model of RPM-FS machine in PM coordinate. (a) PM-MMF vs. mechanical position. (b) Stator air-gap permeance vs. mechanical position.

Hence, the no-load air-gap flux density $B_{gap}(\theta, t)$ of the RPM-FS machine under open-circuit condition can be calculated as:

$$B_{gap}(\theta,t)=\Lambda_{S0}\sum_{n=1}^{\infty}F_{RPMn}\sin(nP_{PM}\theta)+\frac{1}{2}\sum_{n=1}^{\infty}\sum_{k=1}^{\infty}F_{RPMn}\Lambda_{Sk}(\sin\alpha_1+\sin\alpha_2) \tag{4}$$

where

$$\begin{cases}\alpha_1=(nP_{PM}+kP_s)\theta+kP_s(\omega_{r\_PM}t+\theta_0)\\ \alpha_2=(nP_{PM}-kP_s)\theta-kP_s(\omega_{r\_PM}t+\theta_0)\end{cases}$$

It can be found from equation (4) that the open-circuit air-gap flux density is composed of harmonics with nP_{PM} orders and $|nP_{PM}\pm kP_s|$ orders. The harmonics with nP_{PM} orders are produced by the PM-MMF only, which is relatively static in the PM coordinate system. However, for the harmonics with $|nP_{PM}\pm kP_s|$ orders due to the modulation effect by the salient stator teeth, the corresponding harmonic frequency is $kP_sf_{\_PM}$ ($f_{\_PM}=n_b/60$ is fundamental mechanical frequency, and n_b is the rated speed), which will produce the P_{PMloss}. In addition, comparing the harmonic analysis results by the conventional stator coordinate system [4] with those by the PM coordinate system in this paper, the resulting harmonic orders are identical, while the corresponding harmonics rotation speed and frequency are different as listed in Table I. For example, the rotation speeds of the harmonics with nP_{PM} orders are $nP_{PM}\omega_{r\_PM}$ and 0 in the conventional stator coordinate system and the PM coordinate system, respectively.

The open-circuit PM air-gap flux density harmonics distribution is shown in Fig. 3. It can be found that the harmonics with 10th and 50th orders are produced by the fundamental PM-MMF, i.e. $v=nP_{PM}$, n=1 and 5, and the corresponding frequency f_{v_PM}=0. Meanwhile, the dominant modulation harmonics are 14- and 34-pole-pairs in air gap field, i.e. $v=|nP_{PM}\pm kP_s|$, n=1, k=1, and the frequency is $f_{v\_PM}=24f_{\_PM}$.

TABLE I
NO-LOAD PM FIELD HARMONICS OF RPM-FS MACHINE IN PM COORDINATE

Harmonic orders	Rotation speed	Frequency
nP_{PM}	0	0
$\|nP_{PM}\pm kP_s\|$	$kP_s\omega_{r\_PM}/\|nP_{PM}\pm kP_s\|$	$kP_sf_{\_PM}$

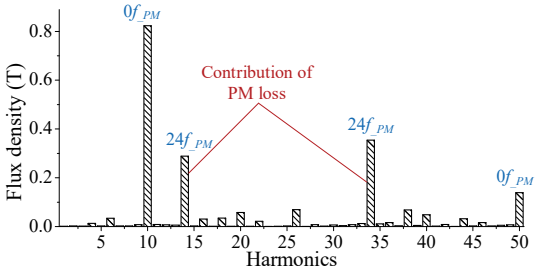

Fig. 3 The open-circuit PM air-gap flux density harmonics distribution of the RPM-FS machine.

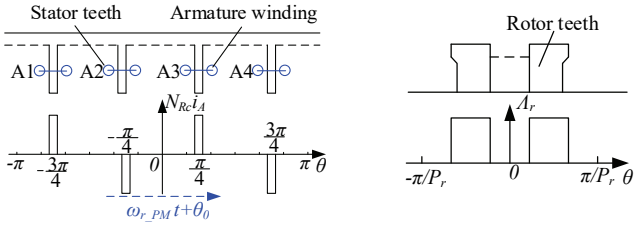

Fig. 4 The armature reaction-MMF/permeance model of RPM-FS machine in the PM coordinate. (a) Armature reaction-MMF vs. mechanical position. (b) Rotor air-gap permeance vs. mechanical position.

On the other hand, the armature reaction-MMF also rotates by an angular speed ω_{r_PM} in PM coordinate system as shown in Fig. 4, which can be expressed as equations (5).

$$\begin{cases}F_{Rw}(\theta,t)=\dfrac{12N_{Rc}I_{R\max}}{\pi}\displaystyle\sum_{i=1}^{\infty}F_{Rwi}\cos\xi\\ \xi=\begin{cases}(4i-2)(\theta+\theta_0)+[P_r+(4i-2)]\omega_{r\_PM}t+\pi, & i=3r-2\\ (4i-2)(\theta+\theta_0)-[P_r-(4i-2)]\omega_{r\_PM}t, & i=3r\end{cases}\end{cases} \tag{5}$$

where N_{Rc} is coil turns number in RPM-FS machine, I_{Rmax} is the maximum value of phase current, F_{Rwi} is the Fourier coefficients of armature reaction-MMF. P_r is the rotor pole pairs number, which is equal to the PM pole pairs number in RPM-FS machine, i.e. $P_r=P_{PM}$=10. r is equal to 1, 2, 3…

The rotor air-gap permeance without taking PMs into consideration can be expressed by equation (6), which is static in PM coordinate system.

$$\Lambda_{Rr}(\theta)=\Lambda_{Rr0}+\sum_{p=1}^{\infty}\Lambda_{Rrp}\cos(pP_r\theta) \tag{6}$$

where Λ_{Rr0} and Λ_{Rrp} are the Fourier series coefficients, p is 1, 2, 3…

Therefore, the armature reaction air-gap flux density $B_{Rw}(\theta,t)$ can be obtained

$$\begin{cases}B_{Rw}(\theta,t)=\dfrac{12N_{Rc}}{\pi}\Lambda_{Rr0}I_{R\max}\displaystyle\sum_{i=1}^{\infty}F_{Rwi}\cos\xi\\ \qquad\qquad+\dfrac{6N_{Rc}}{\pi}I_{R\max}\displaystyle\sum_{i=1}^{\infty}\sum_{p=1}^{\infty}F_{Rwi}\Lambda_{Rrp}\cos\beta_1+\cos\beta_2\\ \beta_1=\begin{cases}(4i-2+pP_r)\theta+(4i-2)\theta_0+(4i-2+P_r)\omega_{r\_PM}t+\pi, & i=3r-2\\ (4i-2+pP_r)\theta+(4i-2)\theta_0+(4i-2-P_r)\omega_{r\_PM}t, & i=3r\end{cases}\\ \beta_2=\begin{cases}(4i-2-pP_r)\theta+(4i-2)\theta_0+(4i-2+P_r)\omega_{r\_PM}t+\pi, & i=3r-2\\ (4i-2-pP_r)\theta+(4i-2)\theta_0+(4i-2-P_r)\omega_{r\_PM}t, & i=3r\end{cases}\end{cases} \tag{7}$$

From equations (7), the armature reaction air-gap flux density harmonics are summarized in Table II. It can be found

This article has been accepted for publication in a future issue of this journal, but has not been fully edited. Content may change prior to final publication. Citation information: DOI 10.1109/TIE.2019.2902782, IEEE Transactions on Industrial Electronics

that the dominant harmonic components of armature reaction-MMF are 4i-2 orders, whereas the harmonics with |4i-2±pP_r| orders are generated by the modulation of the salient rotor cores. It is worth noting that PM eddy current loss is mainly contributed by the harmonic components (HCs) yield,

$$\begin{cases} HC \neq 4i-2, i=3 \\ HC \neq 4i-2 \pm pP_r, i=3 \end{cases} \tag{8}$$

TABLE II
ARMATURE-REACTION FIELD HARMONICS OF RPM-FS MACHINE IN PM COORDINATE

i	Harmonic orders	Rotation speed	Frequency
i=3r-2	4i-2	(4i-2+P_r)ω_{r_PM}/(4i-2)	(4i-2+P_r)$f_{\_PM}$
	4i-2±pP_r	(4i-2+P_r)ω_{r_PM}/(4i-2±pP_r)	(4i-2+P_r) $f_{\_PM}$
i=3r	4i-2	(4i-2-P_r)ω_{r_PM}/(4i-2)	(4i-2-P_r) $f_{\_PM}$
	4i-2±pP_r	(4i-2-P_r)ω_{r_PM}/(4i-2±pP_r)	(4i-2-P_r) $f_{\_PM}$

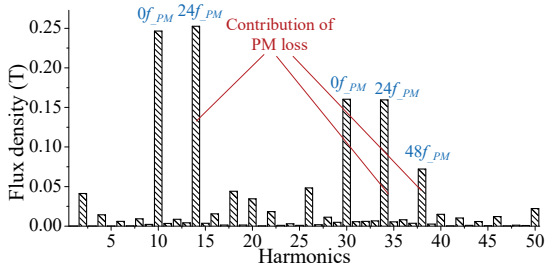

Fig. 5 The armature reaction air-gap flux density harmonics distribution of the RPM-FS machine.

The armature reaction flux density harmonics distribution in the air-gap is shown in Fig. 5. Obviously, the harmonic components generated by the armature reaction MMF are 10th, 14th, 34th, and 38th orders, i.e. 4i-2 (i=3, 4, 9, 10), whereas the harmonic with 30th order is generated by the modulation effect, i.e. 4i-2+pP_r (i=3, p=2). Briefly, the frequencies of 10th/30th harmonics are 0 due to i=3, which is static relative to PMs. The frequencies of the harmonics with 14th/34th orders are 24$f_{_PM}$, whereas 48$f_{_PM}$ for the 38th order as well.

B. SPM-FS machine.

For the SPM-FS machine, the PM-MMF and armature reaction-MMF are also modulated by the salient rotor teeth in air-gap field. Since the PMs are mounted in the stator and static in the stator coordinate system, the MMF/permeance model based on the PM coordinate system are the same as that on the traditional stator coordinate system as shown in Fig. 6 [9].

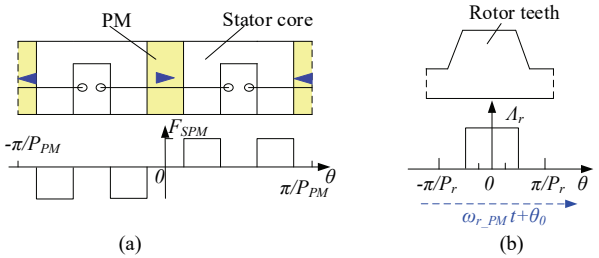

Fig. 6 The PM-MMF permeance model of SPM-FS machine. (a) PM-MMF vs. mechanical position. (b) Rotor air-gap permeance vs. mechanical position.

The open-circuit PM flux density harmonics in air-gap can be deduced as listed in Table III, including those with nP_{PM} order by the PM-MMF only (n=1, 3...), and |nP_{PM}±kP_r| orders due to the modulation effect of salient rotor teeth to PM air-gap field (k=1, 2…). The frequencies of harmonics with nP_{PM} orders are 0 due to the static PMs in the coordinate system. Hence, P_{PMloss} under the open-circuit condition is dominantly generated by the modulated harmonics with |nP_{PM}±kP_r| orders and the frequencies of $kP_rf_{\_PM}$.

TABLE III
NO-LOAD PM FIELD HARMONICS OF SPM-FS MACHINE

Harmonic orders	Rotation Speed	Frequency
nP_{PM}	0	0
|nP_{PM}±kP_r|	$kP_r\omega_{r\_PM}$/[nP_{PM}±kP_r]	$kP_rf_{\_PM}$

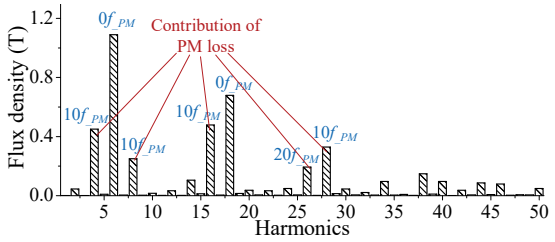

Fig. 7 Open circuit-PM air-gap flux density harmonics distribution of the SPM-FS machine.

The distribution of the open-circuit PM air-gap flux density harmonics is shown in Fig. 7. The dominant harmonics with 6th and 18th orders (v=nP_{PM}, n=1, 3) are produced by the fundamental PM-MMF, and the corresponding frequencies f_{v_PM} are 0. Nevertheless, the frequencies of modulated harmonics with 4th, 8th, 16th and 28th orders (v=|nP_{PM}±kP_r|, n=1, 3 and k=1) are 10$f_{_PM}$, and the harmonics with 26th order (v=|nP_{PM}+kP_r|, n=1 and k=2) is 20$f_{_PM}$.

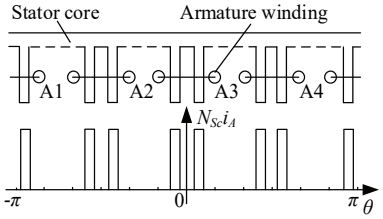

Fig. 8 The armature reaction-MMF model of the SPM-FS machine.

Since the armature reaction-MMF is also modulated by the salient rotor cores, the MMF/permeance model of the SPM-FS machine is shown in Fig. 8, and the harmonic distributions of the modulated armature reaction-field are listed in Table IV. The fundamental components of armature reaction-MMF can be determined as 4i (i=1, 2… without the multiples of three orders), and the frequency is $P_rf_{\_PM}$. Further, taking the modulation effect into consideration, the modulated harmonics of armature reaction air-gap field are defined as |4i±pP_r| (p=1, 2…), and the corresponding frequencies are (p±1)$P_rf_{\_PM}$. It is found that the PM eddy current loss is dominantly generated by the HCs satisfying equation (9), where r is 1, 2, 3…

$$\begin{cases} HC \neq 4i-P_r, i=3r-2 \\ HC \neq 4i+P_r, i=3r-1 \end{cases} \tag{9}$$

The air-gap flux density of the modulated armature reaction

This article has been accepted for publication in a future issue of this journal, but has not been fully edited. Content may change prior to final publication. Citation information: DOI 10.1109/TIE.2019.2902782, IEEE Transactions on Industrial Electronics

field is shown in Fig. 9. The dominant harmonics are 4-, 6-, 8-, 14-, 16- and 20-pole-pairs, where the 4th, 8th, 16th and 20th orders are generated due to the armature reaction-MMF directly (v=4i, i=1, 2, 4, 5), whereas the 6th and 14th harmonic orders are produced by the modulation effect of salient rotor core (v=|4i±pP_r|, i=p=1). Based on the frequency calculated, the P_{PMloss} is mainly attributed by the harmonics with 4th, 8th, 16th and 20th orders, i.e. f_{v_PM} =10$f_{_PM}$, and 14th order i.e. f_{v_PM} =20$f_{_PM}$.

TABLE IV
ARMATURE REACTION FIELD HARMONICS OF SPM-FS MACHINE

i	Harmonic orders	Rotation speed	Frequency
i=3r-2	4i	$P_r\omega_{r\_PM}$/4i	$P_rf_{\_PM}$
	|4i±pP_r|	(p±1)$P_r\omega_{r\_PM}$/(4i±pP_r)	(p±1)$P_rf_{\_PM}$
i=3r-1	4i	-$P_r\omega_{r\_PM}$/4i	$P_rf_{\_PM}$
	|4i±pP_r|	(p±1)$P_r\omega_{r\_PM}$/(4i±pP_r)	(p±1)$P_rf_{\_PM}$

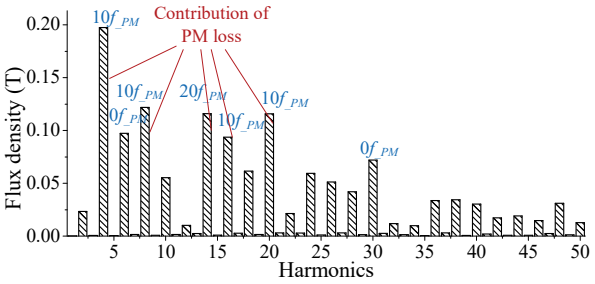

Fig. 9 The armature reaction air-gap flux density harmonics distribution of SPM-FS machine.

III. PM LOSS COMPARISON IN FS MACHINES

Based on the air-gap field harmonics analysis, the effective harmonic orders and frequencies f_{v_PM} producing P_{PMloss} have been revealed above. In this section, P_{PMloss} in two FS machines are predicted and compared under no-load and on-load conditions, whose key parameters are listed in Fig. 10 and Table V.

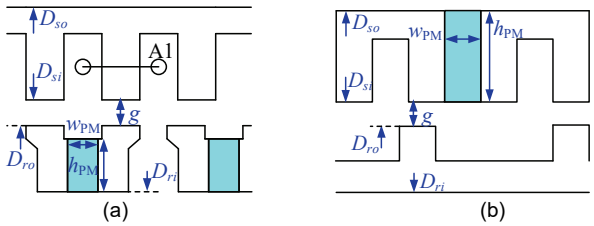

Fig. 10 Key parameters of two FS machines. (a) RPM-FS machine. (b) SPM-FS machine.

TABLE V
KEY PARAMETERS OF TWO FLUX SWITCHING MACHINES

Items	RPM-FS	SPM-FS
P_s/P_r	24s/10p	12s/10p
Stack length l_a (mm)	75	
Stator outer diameter D_{so} (mm)	128	
Stator inner diameter D_{si} (mm)	76.8	70.4
Air gap length g (mm)	0.35	
Rotor outer diameter D_{ro} (mm)	76.1	69.7
Rotor inner diameter D_{ri} (mm)	50.7	22
PM width w_{PM} (mm)	4.54	4.6
PM height h_{PM} (mm)	10.62	28.8
Iron lamination type	50WW470	
Permanent magnet type	N35SH	

A. Open-circuit no-load condition

For doubly salient FS machines, the air-gap permeance varies periodically as the rotor rotates, resulting in a periodic PM flux density, and consequently open-circuit PM eddy current loss.

For the PM air-gap field, the PM-MMF are modulated by the salient iron core P_t, where the P_t is equal to P_s in RPM-FS and P_r in SPM-FS machines, respectively. Then, the harmonics in air gap field is determined as v=|nP_{PM}±kP_t|, and the frequency f_{v_PM} is $kPf_{\_PM}$ (n=1, 2…, k=0, 1, 2…). It is worth noting that only the modulated harmonic components |nP_{PM}±kP_t| orders (k≠0) contribute the open-circuit P_{PMloss} since the harmonics frequency f_{v_PM}≠0.

The PM flux density distributions of two FS machines are predicted by FEA in Figs. 11 and 12. For the RPM-FS machine, the dominant harmonics with frequency of 24$f_{_PM}$ in Fig. 11(b) is caused by the air-gap field modulation harmonics with 14th and 34th orders as derived above, which generate P_{PMloss}. Similarly, P_{PMloss} in the SPM-FS machine is dominantly contributed by the modulated harmonics with 4th, 8th, 16th, 26th and 28th orders, and the corresponding frequency can be deduced to be 10$kf_{_PM}$ (k=1, 2), which is also verified by the harmonics distribution of PM flux density as shown in Fig. 12(b).

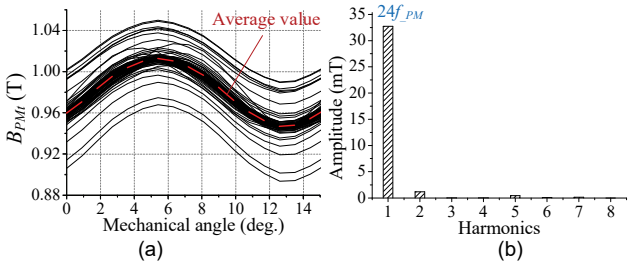

Fig. 11 The open-circuit PM flux density of the RPM-FS machine. (a) PM elements flux density distribution. (b) The harmonics distribution.

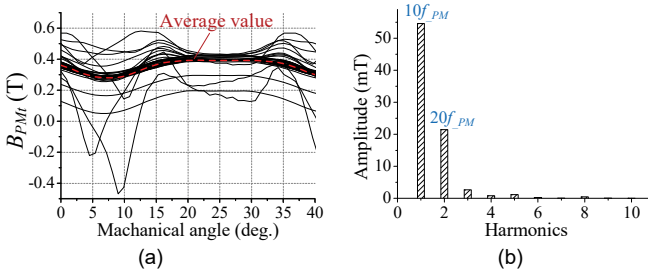

Fig. 12 The open-circuit PM flux density of the SPM-FS machine. (a) PM elements flux density distribution. (b) The harmonics distribution.

The open-circuit PM eddy current loss density $k_{PMloss/V}$ (the ratio of P_{PMloss} to PM volume) at base speed (n_b=1500r/min) by equation (1) and 3D-FEA are shown in Fig. 13. It can be found that the analytical results by equation (1) are slightly higher than the 3D-FEA results. The reasons can be attributed to two perspectives. (1) The flux densities are assumed to be the squared waveforms and distribute uniformly in the PMs of machines for the PM eddy current loss calculation. (2) The analytical model in equation (1) only considers the flux density along the PM magnetized direction, i.e. eddy current parallel to

This article has been accepted for publication in a future issue of this journal, but has not been fully edited. Content may change prior to final publication. Citation information: DOI 10.1109/TIE.2019.2902782, IEEE Transactions on Industrial Electronics

the PM plane (the PM plane is perpendicular to the PM magnetized direction), and the eddy current along the PM magnetized direction is neglected. The analytical PM eddy current loss of SPM-FS machine is 2.03×10^{-4}W/mm^2, which is 9% higher than that of 3D-FEA result. For the RPM-FS machine, the PM loss error of RPM-FS machine between analytical result and 3D-FEA result is 11%. In addition, the $k_{PMloss/V}$ of SPM-FS machine by 3D-FEA (1.85×10^{-4}W/mm^3) is significantly higher than that of the RPM-FS machine (2.4×10^{-5}W/mm^3). In addition, $k_{PMloss/V}$ from equation (1) is mainly influenced by the geometric parameters of PM, and hence it can be expected that PM segmentation is helpful to reduce the PM eddy current loss. For the SPM-FS machine with 3 PM segmentations (SPM-FS_3), the geometric parameters of the segmental PM are approximately identical to those of the RPM-FS machine. Consequently, the $k_{PMloss/V}$ of SPM-FS_3 is 3.19×10^{-5}W/mm^3, which is 1.3 times of the RPM-FS machine, since B_{smv} of the SPM-FS machine in Fig. 12(b) is larger than that of the RPM-FS machine in Fig. 11(b).

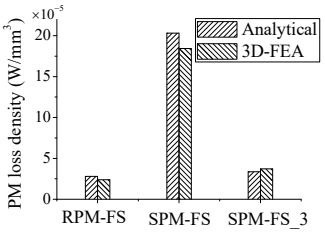

Fig. 13 The analytically predicted and FEA predicted open-circuit PM loss densities in FS machines with different topologies at n_b=1500r/min.

B. Rated on-load condition

The harmonics of armature reaction field in two FS machines can be determined as $|HC\pm pP_r|$ (p=0, 1, 2…), where the HCs are $4i$-2 and $4i$ (i=1, 2… and HCs without the multiples of three orders) in the RPM-FS and the SPM-FS machine, respectively. For the SPM-FS machine, the PMs and armature windings are both in the stator and relatively static, thus the harmonics frequency is $|p\pm1|P_rf_{\_PM}$ (p=0, 1, 2…). However, the harmonics $|HC\pm pP_r|$ frequencies of RPM-FS machine are $|HC\pm P_r|f_{\_PM}$, since the PMs mount in the rotor, which results in the rotating of the PM field relative to the armature reaction field.

The flux density variation in PMs of two machines at J_{sa_rms}=5A/mm^2 and n_b=1500r/min are shown in Figs. 14 and 15. It can be found that the dominant harmonics frequencies of flux density in PMs in RPM-FS machine are $12f_{\_PM}$ and $24f_{\_PM}$ as shown in Fig. 14(b), which is attributed by the armature reaction harmonics with 14th, 34th and 38th orders, and then the PM eddy current loss is generated. For the SPM-FS machine, the flux density harmonics in PMs with $10f_{\_PM}$ and $20f_{\_PM}$ shown in Fig. 15(b) are contributed by the dominant harmonics of armature reaction field with 4th, 8th, 14th, 16th and 20th orders.

Correspondingly, the rated on-load $k_{PMloss/V}$ at J_{sa_rms}=5A/mm^2 and n_b=1500r/min of two FS machines are compared in Fig. 16, and overall the agreements between the analytical and 3D-FEA results are well. The analytical PM eddy current loss density of SPM-FS machine is 2.1×10^{-4}W/mm^2, which is 4% higher than that of 3D-FEA result. For the RPM-FS machine, the PM loss by equation (1) is 1.14 times of that of 3D-FEA result. Moreover, the $k_{PMloss/V}$=7.73×10^{-5}W/mm^3 at rated on-load condition by 3D-FEA is 3.2 times of that under the open-circuit condition of the RPM-FS machine. However, for the SPM-FS machine without PM segmentation, $k_{PMloss/V}$ increases only by 8% under the rated on-load condition ($k_{PMloss/V}$=2.01×10^{-4}W/mm^3). It can be concluded that the $k_{PMloss/V}$ in RPM-FS machine is more sensitively influenced by the armature reaction field than the SPM-FS machine. The reason is that both PMs and armature windings coexist in the stator of the SPM-FS machine, which leads to a lower electrical loading, and the PM field is hardly influenced by the armature reaction field as shown in Figs. 12(b) and 15(b). In addition, the PM loss ratio k_{PMloss} (the ratio of PM loss to output power) of the SPM-FS machine without PM segmentation is 1.1%, which is 10 times of the RPM-FS machine (0.11%). Moreover, for the SPM-FS_3 machine with 3 PM segmentations, the $k_{PMloss/V}$ is significantly reduced, i.e. $k_{PMloss/V}$=3.23×10^{-5}W/mm^3, which is about 42% of the RPM-FS machine with the similar PM geometric dimensions as shown in Table VI. The reason is that the $20f_{\_PM}$ harmonic amplitude and frequency in PM flux density of the SPM-FS machine is significantly lower than the $24f_{\_PM}$ harmonic in the RPM-FS machine, as shown in Figs. 14(b) and 15(b), respectively.

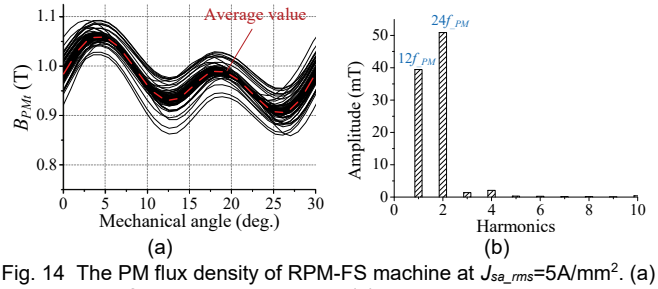

Fig. 14 The PM flux density of RPM-FS machine at J_{sa_rms}=5A/mm^2. (a) PM elements flux density distribution. (b) The harmonics distribution.

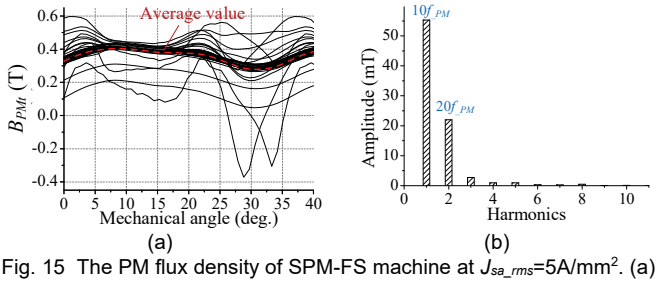

Fig. 15 The PM flux density of SPM-FS machine at J_{sa_rms}=5A/mm^2. (a) PM elements flux density distribution. (b) The harmonics distribution.

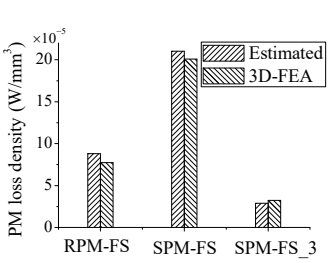

Fig. 16 The analytically predicted and FEA predicted PM loss densities in FS machines with different topologies at J_{sa_rms}=5A/mm^2 and n_b=1500r/min.

This article has been accepted for publication in a future issue of this journal, but has not been fully edited. Content may change prior to final publication. Citation information: DOI 10.1109/TIE.2019.2902782, IEEE Transactions on Industrial Electronics

TABLE VI
PREDICTED PERFORMANCES OF THREE FS MACHINES BY 3D-FEA

Items	RPM-FS	SPM-FS	SPM-FS_3
Rated current density (A/mm^2)		5	
Base speed n_b (r/min)		1500	
Output torque (Nm)	15.5		13.1
Output power (W)	2434		2057
PM volume (mm^3)	3.3×10^4		1.2×10^5
PM loss P_{PMloss} (W)	2.58	24	3.85
PM loss density $k_{PMloss/V}$ (W/mm^3)	7.73×10^{-5}	2.01×10^{-4}	3.23×10^{-5}
PM loss ratio k_{PMloss}	0.11%	1.1%	0.19%

Based on the gearing effect, the electromagnetic torque of RPM-FS machines and SPM-FS machines are produced by the interaction of the magnetic loading harmonics and the electrical loading harmonics with the same order and rotating speed in the air gap field [6], [9]. Hence, the electromagnetic torque can be expressed as [4]:

$$T_e = \frac{\pi}{4} D_{so}^2 l_a \sum_v B_{gv} A_{Wv} \cos\phi_v k_{sio}^2 \quad (10)$$

where, φ_v is the v-order harmonic angle between magnetic loading B_{gv} and electrical loading A_{wv}, k_{sio} is the split ratio (the ratio of stator inner diameter and stator outer diameter for inner-rotor machines). The harmonics proportions of two FS machines are shown in Fig. 17. It can be seen that T_e of RPM-FS machine T_{e_RPM} is dominantly contributed by the fundamental component, i.e. v=P_{PM}=10th harmonic order (83%), and the PM eddy current loss is produced by the modulated harmonics $|nP_{PM}\pm kP_s|$ (n=k=1), e.g. 14th and 34th harmonic orders. However, for the SPM-FS machine, T_{e_SPM} is mainly generated by the modulated harmonics $|nP_{PM}\pm kP_r|$ (n=1, 3, k=1), including harmonics with 4th (28.5%), 8th (-14%), 16th (29.2%) and 28th (9.5%), which also results in P_{PMloss}. In general, the characteristics differences between RPM-FS and SPM-FS machines are not only in electromagnetic torque production mechanism and but also in PM eddy current loss generation mechanism.

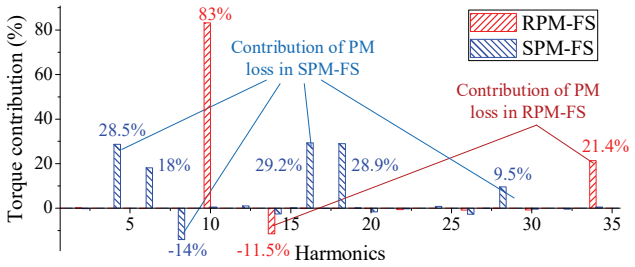

Fig. 17 Electromagnetic torque contributions due to dominant harmonic components in the RPM-FS and SPM-FS machines.

From equation (10), it can be found that the torque is mainly determined by k_{sio} when two machines have the same D_{so} and l_a as listed in Table V. Hence, T_e vs. k_{sio} characteristics of two machines at J_{sa_rms}=5A/mm^2 are shown in Fig. 18, where the maximum torque of the RPM-FS and SPM-FS machines is obtained at k_{sio}=0.6 and 0.55, respectively.

On the other hand, according to the above PM segmentation analysis, the $k_{PMloss/V}$ is significantly influenced by the PM height h_{PM}. For the SPM-FS machine, h_{PM} is only determined by split ratio k_{sio}, while for the RPM-FS machine h_{PM} can be optimized by k_{sio} and rotor teeth height ratio k_{hrt} (the ratio of D_{ro} to D_{ri}). Hence, the h_{PM} of SPM-FS machine is always larger than that of RPM-FS machine with the same D_{so} at the low power rating machine design with low current density, e.g. J_{sa_rms}=5A/mm^2, which results in a higher $k_{PMloss/V}$ and k_{PMloss}.

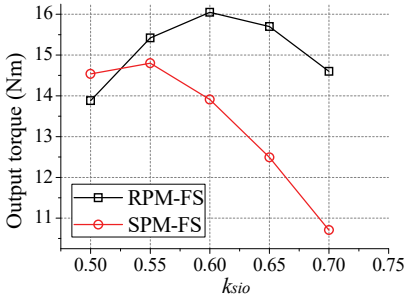

Fig. 18 The output torque vs. k_{sio} of two FS machine at J_{sa_rms}=5A/mm^2.

C. Experimental Verifications

To verify the above analysis, two prototyped FS machines are manufactured as shown in Fig. 19. Fig. 20 shows the analytical, 3D-FEA and measured output torque vs. current densities of two machines, where the analytical torque is the electromagnetic torque only considering the dominant harmonics contribution shown in Fig. 17. For the RPM-FS machine, the electromagnetic torque contributed by the harmonics with 10th, 14th and 34th orders is 14.86Nm, which is about 92.6% of the total torque by 2D-FEA (16.05Nm) at J_{sa_rms}=5A/mm^2. Hence, it can be concluded that the electromagnetic torque is mainly produced by the harmonics with 10th, 14th and 34th orders. In addition, considering the flux leakage along the axial direction, i.e., the end-effect, the resultant 3D-FEA result is 15.5Nm, which is so close to the measured torque of the RPM-FS machine (15Nm at 5A/mm^2).

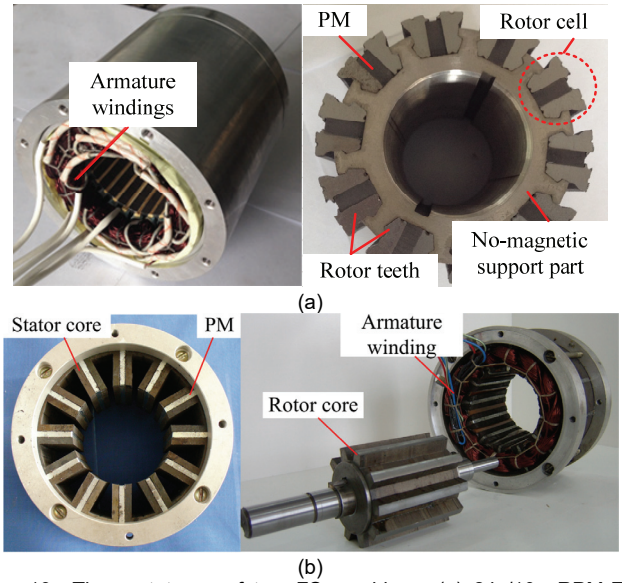

Fig. 19 The prototypes of two FS machines. (a) 24s/10p RPM-FS machine. (b) 12s/10p SPM-FS machine.

For the SPM-FS machine, the electromagnetic torque is dominantly contributed by the harmonics with 4th, 6th, 8th, 16th, 18th, and 28th orders as shown in Fig. 17. The electromagnetic torque at J_{sa_rms}=5A/mm^2 produced by the

This article has been accepted for publication in a future issue of this journal, but has not been fully edited. Content may change prior to final publication. Citation information: DOI 10.1109/TIE.2019.2902782, IEEE Transactions on Industrial Electronics

dominant harmonics is 14.65Nm, which is about 99% of that of 2D FEA as shown in Fig. 20(b). Moreover, considering the end-effect, the 3D-FEA prediction is 13.05Nm, and the measured total torque of the SPM-FS machine is 12.42Nm at 5A/mm^2. The error between measured and 3D FEA predicted results can be attributed to the manufacturing tolerances and assembling process.

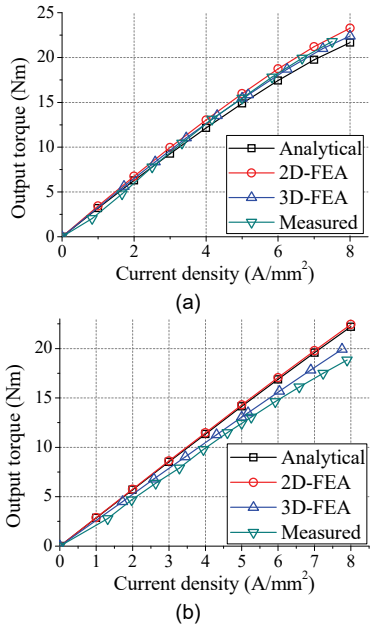

Fig. 20 Measured and predicted output torque vs. current densities. (a) RPM-FS machine. (b) SPM-FS machine.

The efficiencies by 3D-FEA of two machines are slightly higher than the measured results as shown in Fig. 21. For example, the measured efficiency of the RPM-FS machine at rated 5A/mm^2 is 86.3%, which is 0.7% lower than the 3D-FEA result. For the SPM-FS machine, a reduction of 0.9% of the measured efficiency (86.34%) is obtained compared with the 3D-FEA result.

At the low current density conditions, the copper loss ratio $k_{copperloss}$ (the ratio of copper loss to output power) is lower in the FS machines, whereas the PM loss and core loss are the dominant loss components and influence the efficiency dramatically. For instance, the copper loss of SPM-FS machine at J_{sa_rms}=2A/mm^2 is 15.35W, which is about 3.2% of the output power, i.e. $k_{copperloss}$=3.2%. However, the sum of PM loss and core loss is 39.6W, which is 8.3% of the output power. Hence, the efficiency of SPM-FS machine is significantly determined by the PM loss and core loss. Similarly, the copper loss and the sum of PM loss and core loss of RPM-FS machine at J_{sa_rms}=2A/mm^2 are 3.6% and 4.2% of the output power, respectively. The efficiency of RPM-FS machine at J_{sa_rms}=2A/mm^2 is 88% by 3D-FEA, which is higher than that of SPM-FS machine (85.2%). The reasons are that the core loss of two machines are approximately identical (27W), whereas the PM loss ratio of RPM-FS machine is only 0.1%, which is significantly lower than that of SPM-FS machine (2.6%). In addition, the measured efficiency of RPM-FS machine (85%) is higher than that of SPM-FS machine (83.7%) at J_{sa_rms}=2A/mm^2, which verifies the above analysis.

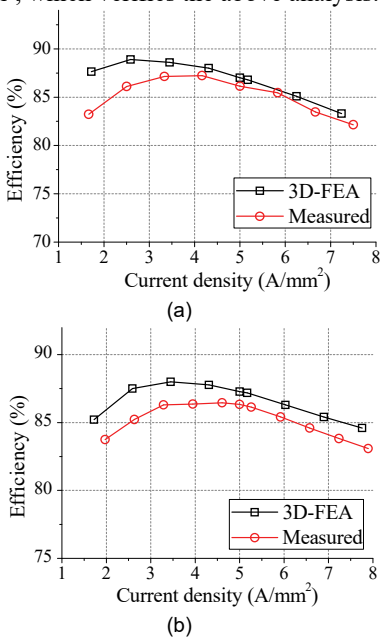

Fig. 21 Measured and predicted efficiencies vs current densities. (a) RPM-FS machine. (b) SPM-FS machine.

IV. PM LOSS IN HIGH-POWER RATING FS MACHINES

For the driving machines utilized in PEVs and HEVs, key characteristics are desired, including large power (torque) density, wide speed regulation range, and high efficiency in a whole operation range [14]. These required performances cause large current density and high fundamental frequency, which further influence B_{smv} and ω_{v_PM} in equation (1), and then a significant improvement of $k_{PMloss/V}$ is obtained. Hence, the efficiency of driving machines is influenced by the P_{PMloss} dramatically, which should be analyzed further.

Two FS machines for EV and HEV applications have been designed in [5] with the same outside diameter D_{so} and effective axial length l_a, as shown in Table VII. The maximum current density J_{samax}=20.8A/mm^2 and base speed n_b is 1200r/min. The PM operation temperature is assumed as 120ºC at the maximum torque operation condition. The combinations of P_s/P_r for high-power rating and large current density RPM-FS and SPM-FS machines are the same as low-power rating machines, hence the air-gap harmonics distributions of modulated PM-MMF and armature reaction-MMF are the same. Then the effective harmonics contributing to the PM eddy current loss in high-power rating machines are identical as analyzed in Section II.

To design FS machines with 20.8A/mm^2 employing a liquid-cooling system, stator teeth saturation is more serious than the case of 5A/mm^2. Hence, a high k_{sio} is chosen, which results in a wider stator teeth width, and then the stator teeth saturation can be alleviated, being helpful to improve the torque capability. Fig. 22 shows the output torque vs. k_{sio} of two FS machines at 20.8A/mm^2. The optimized k_{sio} of the RPM-FS machine and SPM-FS machines are the same as 0.7. Meanwhile, the PMs and armature windings co-exist in stator, the

This article has been accepted for publication in a future issue of this journal, but has not been fully edited. Content may change prior to final publication. Citation information: DOI 10.1109/TIE.2019.2902782, IEEE Transactions on Industrial Electronics

reductions of electrical loading and magnetic loading are obtained in the SPM-FS machine with k_{sio}=0.7. Hence, the T_e of the SPM-FS machine (305Nm) is 88% of the RPM-FS machine (347Nm), and the torque density is 22% lower than the RPM-FS machine. For the RPM-FS machine, the electrical loading also decreases as k_{sio} increases, whereas the magnetic loading can be improved by adjusting the PM height h_{PM}, and then the machine exhibits a higher torque capability and an increased $k_{PMloss/V}$.

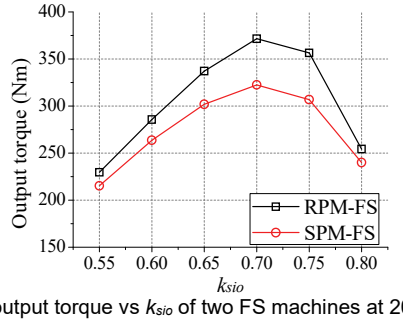

Fig. 22 The output torque vs k_{sio} of two FS machines at 20.8A/mm^2.

TABLE VII
DIMENSIONS AND PERFORMANCES OF TWO FS MACHINES BY 3D-FEA.

Items	RPM-FS	SPM-FS
P_s/P_r	24s/10p	12s/10p
Stack length l_a	83.56	
Stator outer diameter D_{so} (mm)	269	
Stator inner diameter D_{si} (mm)	193.7	195.8
Air gap length g (mm)	0.73	
Rotor outer diameter D_{ro} (mm)	192.2	194.4
Rotor inner diameter D_{ri} (mm)	124.9	110
PM width w_{PM} (mm)	12.89	10.25
PM height h_{PM} (mm)	31.64	36.58
Iron lamination type and PM-type	M19_29G, N36Z_20	
Maximum current density (A/mm^2)	20.8	
PM volume (mm^3)	340790	375965
PM mass (kg)	2.57	2.84
Total mass (kg)	30.3	33.9
Maximum torque (Nm)	347.2	305.7
Torque density (Nm/kg)	11.5	9.0
Base speed n_b (r/min)	1200	
Output power (W)	43627	38412
Power density (kW/kg)	1.4	1.1
PM loss P_{PMloss} (W)	789	685.4
PM loss density $k_{PM/V}$ (W/mm^3)	2.23×10^{-3}	1.83×10^{-3}
PM loss ratio k_{PMloss}	1.8%	1.8%
Copper loss (W)	4405	4594
Core loss (W)	257	225
Efficiency	87.3%	85.2%
Power factor	0.74	0.76

In addition, the $k_{PMloss/V}$ is dominantly determined by h_{PM} in above analysis. For the SPM-FS machine with high power rating and large current density, the PM height ratio k_{hPM} (the ratio of h_{PM} to D_{so}/2) is 0.27, which is 60% of the low power rating and current density case (k_{hPM}=0.45), due to an enlarged k_{sio}. Taking the improvement of harmonic amplitudes B_{smv} in Fig. 23 into consideration, the $k_{PMloss/V}$ in SPM-FS machines with high power rating and current density design ($k_{PMloss/V}$=1.83×10^{-3}W/mm^3) is 9 times of that case with low power rating and current density. However, the PM height ratio (k_{hPM}=0.24) in RPM-FS machine with large current density is 1.6 times of that case with low current density (k_{hPM}=0.15), which results in a significant increase of $k_{PMloss/V}$. It can be found that the $k_{PMloss/V}$=2.23×10^{-3} W/mm^3 of RPM-FS machine with large current density is 28.8 times of that machine with low current density, which verifies that the $k_{PMloss/V}$ is more significantly influenced by the armature reaction field than the SPM-FS machine. It is worth noting that the $k_{PMloss/V}$ of RPM-FS machine is 1.22 times of that of the SPM-FS machine in high power rating and large current density design, nevertheless, the PM loss ratio of RPM-FS machine (k_{PMloss}=1.8%) is identical to that of SPM-FS machine. Therefore, the P_{PMloss} in both FS machines influences efficiency performance more significantly than that of cases with low current density design, which is dominantly determined by the key parameters of k_{sio} in SPM-FS machines and k_{hrt} in RPM-FS machines. In addition, for the FS machines with high power rating and current density design, the higher PM eddy current loss density is obtained, which results in the rise of PM temperature, and then the magnets demagnetize more easily than the machines with low power rating design. Hence, the PM loss should be reduced by the tangential and axis PM segmentation.

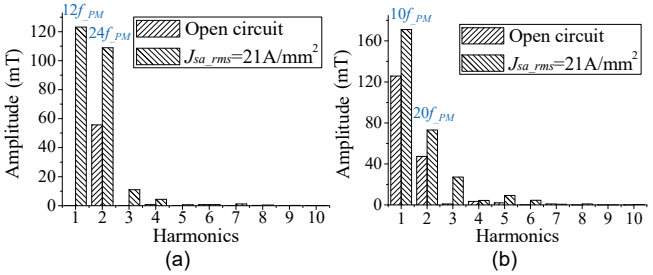

Fig. 23 Harmonic distribution of PM flux density. (a) RPM-FS machine. (b) SPM-FS machine.

Fig. 24(a) shows the $k_{PMloss/V}$ at J_{sa_max}=20.8A/mm^2 and n_b=1200r/min considering the two and three PM radical segmentation configurations. It can be found that 70% and 86% reduction of the $k_{PMloss/V}$ in RPM-FS machine have been obtained by two and three tangential segments per PM, respectively. For the SPM-FS machine, the $k_{PMloss/V}$ without segmentation is 2.8 times and 11.5 times of that case with 2 and 3 segments. In addition, compared with two flux-switching machines with 3 PM segmentations, the $k_{PMloss/V}$ of RPM-FS machine is 2 times of that of the SPM-FS machine.

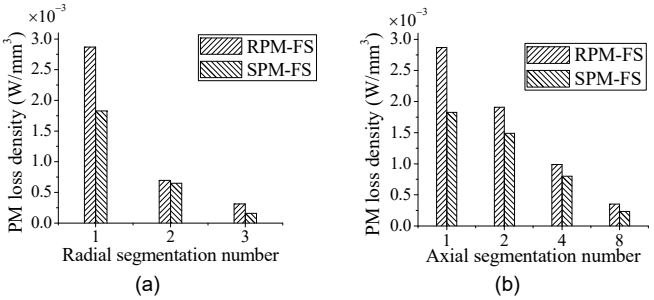

Fig 24 PM loss density vs PM segmentations. (a) Radial direction segmentations. (b) Axial direction segmentations.

The $k_{PMloss/V}$ at J_{samax}=20.8A/mm^2 and n_b=1200r/min utilizing four cases of PM axis segmentations are shown in Fig. 24(b). It can be found that the $k_{PMloss/V}$ in RPM-FS machine with 2, 4 and

8 PM segmentations are 82%, 43% and 15% of that original design, respectively. For the SPM-FS machine, the reductions of $k_{PMloss/V}$ with 2, 4 and 8 PM segmentations are 18%, 56% and 87%. It is worth noting that the radial segmentation exhibits a better effectiveness with respect to the axial one, and the PM with 3 radical segments is chosen as the attractive candidate.

V. Conclusion

This paper investigates the PM eddy current loss in RPM-FS machine and SPM-FS machine, respectively. Based on the field modulation principle, the PM and armature reaction field are modulated by the salient iron cores, which results in a complex harmonics distribution in the air-gap filed. For the RPM-FS machine, the electromagnetic torque is dominantly produced by the fundamental harmonic, while the PM eddy current loss is generated by the modulated harmonics. However, the torque of SPM-FS machine is contributed by the modulated harmonics, which also results in the PM eddy current loss. Therefore, the characteristics difference between two FS machines is not only in the electromagnetic torque production mechanism and but also in the PM eddy current loss generation principle.

On the other hand, the two FS machines are designed and optimized with the same geometric dimensions, base speed and current density to compare the electromagnetic performances. It can be concluded that the output torque of 24s/10p RPM-FS machine is higher than that of 12s/10p SPM-FS machine. In addition, for the SPM-FS machine with low power rating and current density design, the lower k_{sio} is chosen and a significantly longer PM height is obtained, then the PM eddy current loss density and PM loss ratio are larger than those of the RPM-FS machine. However, it is worth noting that PM eddy current loss in RPM-FS machine is more sensitively influenced by the armature reaction field, which is different from that of the SPM-FS machine. In addition, for the FS machines in PEV system with the high power rating and current density, the PM loss densities are increased. Due to the influence of the higher armature reaction field and increased PM height ratio, the PM loss density of RPM-FS machine with high power rating and current density is larger than that of SPM-FS machine, nevertheless, the PM loss ratios of two machines are identical. In general, the PM losses in SPM-FS machines with low and high current density designs influence the efficiency dramatically, whereas PM loss in the RPM-FS machine with only large current density design exhibits a major impact on efficiency.

References

[1] M. Cheng, W. Hua, J. Zhang, and W. Zhao, "Overview of stator-permanent magnet brushless machines," *IEEE Trans. Ind. Electron.*, vol. 58, no. 11, pp. 5087–5101, Nov. 2011.

[2] Zhu, Z. Xiang, C. Zhang, L. Quan, Y. Du, and W. Gu, "Co-reduction of torque ripple for outer rotor flux-switching PM motor using systematic multi-level design and control schemes," *IEEE Trans. Ind. Electron*., vol. 64, no. 2, pp. 1102-1112, Feb. 2017.

[3] D. J. Evans, and Z. Q. Zhu. "Novel partitioned stator switched flux permanent magnet machines." *IEEE Trans. Magn.*, vol. 51, no. 1, pp. 8100114, Jan. 2015.

[4] P. Su, W. Hua, Z.Z. Wu, P. Han, M. Cheng. "Analysis of the operation principle for rotor permanent magnet flux switching machines." *IEEE Trans. Ind. Electro.*, DOI: 10.1109/TIE.2017.2733442.

[5] P. Su, W. Hua, G. Zhang, Z. Chen, M. Cheng. "Analysis and evaluation of novel rotor permanent magnet flux-switching machine for EV and HEV applications." *IET Electr. Power App.*, vol. 11, no. 7, pp.1610-1618, Nov. 2017.

[6] J. D. McFarland, T. M. Jahns, and A. M. EL-Refaie. "Analysis of the torque production mechanism for flux-switching permanent-magnet machines." *IEEE Trans. on Ind. Appl.*, vol. 51, no. 4, pp. 3041-3049, Jul./Aug. 2015.

[7] Y. Shi, L. Jian, J. Wei, W. Li, and C. C. Chan. "A new perspective on the operating principle of flux-switching permanent magnet machines." *IEEE Trans. Ind. Electron.*, vol. 63, no. 3, pp. 1425-1437, Mar. 2016.

[8] M. Cheng, P. Han, W. Hua. "A general airgap field modulation theory for electrical machines." *IEEE Trans. Ind. Electro.*, vol. 64, no. 8, pp. 6063-6074, March. 2017.

[9] Z. Z. Wu, and Z. Q. Zhu, "Analysis of air gap field modulation and magnetic gearing effects in switched flux permanent magnet machines." *IEEE Trans. Magn.*, vol. 51, no. 5, pp. 8105012, May 2015.

[10] M. Cheng, S. Zhu, "Calculation of PM eddy current loss in IPM machine under PWM VSI supply with combined 2-D FE and analytical method." *IEEE Trans. Magn.*, vol. 53, no. 1, pp. 6300112, Jan. 2017.

[11] M. Paradkar and J. Bócker, "3D analytical model for estimation of eddy current losses in the magnets of IPM machine considering the reaction field of the induced eddy currents," in *Proc. IEEE Energy Convers. Congr. Expo. (ECCE)*, Sep. 2015, pp. 2862–2869.

[12] Y. Hu, S. Zhu, and C. Liu. "Magnet eddy-current loss analysis of interior PM machines for electric vehicle application." *IEEE Trans. Magn.*, vol. 53, no.11, Nov. 2017, Art. no. 7402904.

[13] M. Olszewski, "Evaluation of the 2010 Toyota Prius hybrid synergy drive system," U.S. Dept. Energy Vehicle Technol., Washington, DC, USA, Tech. Rep., Mar. 2011, pp. 43–48.

[14] X. Liu, H. Chen, J. Zhao and A. Belahcen, "Research on the performances and parameters of interior PMSM used for electric vehicles". *IEEE Trans. Ind. Electro.*, vol. 63, no. 6, pp. 3533-3545, Feb. 2016.

Peng Su (S'14) was born in Henan, China, in 1988. He received the B.Sc. and M.E. degrees in electrical engineering from Henan Polytechnic University, Henan, China in 2011 and 2013, respectively. Since 2013, he is currently working toward the Ph.D. degree in electrical engineering at Southeast University, Nanjing, China. From December 2016 to December 2017, he was a joint Ph.D. student funded by China Scholarship Council in the Department of Energy Technology, Aalborg University, Aalborg, Denmark.

His current research interests include the design and analysis of novel permanent-magnet brushless electrical machines for application in electric vehicles.

Wei Hua (SM'16) was born in Taizhou, China, in 1978. He received the B.Sc. and Ph.D. degrees in electrical engineering from Southeast University, Nanjing, China, in 2001 and 2007, respectively.

From September 2004 to August 2005, he visited the department of Electronics and Electrical Engineering, The University of Sheffield, UK, as a Joint-Supervised Ph. D student. Since 2007, he has been with Southeast University, where he is currently a Professor with the School of Electrical Engineering. He is the author or coauthor of over 150 technical papers, and he is the holder of 50 patents

in his areas of interest. His teaching and research interests include the design, analysis, and control of electrical machines.

Mingjin Hu received the B.Eng. degree in electrical engineering from the School of Electrical Engineering, Southeast University, Nanjing, China, 2016. Since 2016, he is currently working toward the M.E. degree in electrical engineering at Southeast University, Nanjing, China.

His current research interests include the modeling and advanced control of electrical machines.

Zhe Chen (M'95–SM'98- F'18) received the B.Eng. and M.Sc. degrees all in electrical engineering from Northeast China Institute of Electric Power Engineering, Jilin City, China, in 1982 and 1986, respectively, the M.Phil. degree in power electronic from Staffordshire University, Staffordshire, U.K., in 1993, and the Ph.D. degree in power and control from University of Durham, Durham, U.K., in 1997.

He is a Full Professor with the Department of Energy Technology, Aalborg University, Aalborg, Denmark, since 2002. He is the Danish Principle Investigator for Wind Energy of Sino-Danish Centre for Education and Research and the leader of Wind Power System Research program at the Department of Energy Technology, Aalborg University. He has led many international and national research projects and has more than 500 technical publications with more than 12500 citations (Google Scholar) and h-index of 49. His research interests include power systems, power electronics, and electric machines; and his main current research interests are wind energy and modern power systems.

Dr. Chen is an Associate Editor of the IEEE TRANSACTIONS ON POWER ELECTRONICS, a Fellow of the Institution of Engineering and Technology, London, U.K., and a Chartered Engineer in the U.K.

Ming Cheng (M'01–SM'02–F'15) received the B.Sc. and M.Sc. degrees in Electrical Engineering from the Department of Electrical Engineering, Southeast University, Nanjing, China, in 1982 and 1987, respectively, and the Ph.D. degree in electrical engineering from the University of Hong Kong, Hong Kong, in 2001.

Since 1987, he has been with Southeast University, where he is currently a Distinguished Professor in the School of Electrical Engineering and the Director of the Research Center for Wind Power Generation. From January to April 2011, he was a Visiting Professor with the Wisconsin Electric Machine and Power Electronics Consortium, University of Wisconsin-Madison. His teaching and research interests include electrical machines, motor drives for electric vehicles, and renewable energy generation. He has authored or coauthored over 350 technical papers and 4 books and is the holder of 90 patents in these areas.

Prof. Cheng is a fellow of the Institution of Engineering and Technology. He has served as chair and organizing committee member for many international conferences. He is a Distinguished Lecturer of the IEEE Industry Applications Society (IAS) in 2015/2016.

Wei Wang (S'10-M'14) was born in Jiangsu, China. He received the B.Sc. degree in electrical engineering from Nanjing University of Science & Technology, Nanjing, China, in 2008, and the Ph.D. degree in electrical engineering from Southeast University, Nanjing, China, in 2014, respectively.

Since 2014, he has been with Southeast University, where he is currently an associate professor in the School of Electrical Engineering. From October 2011 to October 2012, he got the scholarship from China Scholarship Council and was a joint Ph.D student with University of Lille 1, Lille, France. He is the author or coauthor of more than 30 technical papers. His research interests include motor drives and traction system for rail transit.